


Article

Research on Fine Estimation of People Trapped after Earthquake on Single Building Level Based on Multi-Source Data

Shizhe Xie ^{1,*}, Dongping Ming ^{1,*} , Jin Yan ^{2,3}, Huaining Yang ², Ran Liu ¹ and Zhi Zhao ¹

¹ School of Information Engineering, China University of Geosciences, Beijing 100083, China; 3004200006@email.cugb.edu.cn (S.X.)

² National Earthquake Response Support Service, Beijing 100049, China

³ College of Resource Environment and Tourism, Capital Normal University, Beijing 100049, China

* Correspondence: mingdp@cugb.edu.cn

Abstract: Risk assessments of people who are trapped are an important basis for scientific and effective emergency rescue after an earthquake. Currently, most models are based on the kilometer grid scale or community scale that gauge the population and extent of the earthquake burial under distinct intensities. The estimation results of the methods are on coarse scales; therefore, the methods cannot meet the requirements of rapid rescue after an earthquake. In response to the above statements, this study uses multi-source data to propose a way to estimate the number and distribution of people trapped under the scale of single buildings. Firstly, we use pre-earthquake optical high spatial resolution remote sensing images for building detection, and then we combine them with multi-source data for population distribution simulation. Secondly, indoor ratio assessment models are constructed by analyzing human behavior. Then, aerial remote sensing images are used for building seismic damage level detection. Finally, based on these three factors, a single building crush burial estimation model is constructed to obtain the number and distribution of personnel trapped. In this paper, the reliability of the proposed workflow is demonstrated by the casualty results in experiments conducted in the nearby Moxi town after the Luding 6.8 magnitude earthquake on 5 September 2022. For future natural disaster events, this method can provide reliable information support and decision references for earthquake emergency rescue.

Keywords: people trapped; multi-source data; distribution evaluation; earthquake emergency rescue



Citation: Xie, S.; Ming, D.; Yan, J.; Yang, H.; Liu, R.; Zhao, Z. Research on Fine Estimation of People Trapped after Earthquake on Single Building Level Based on Multi-Source Data. *Appl. Sci.* **2023**, *13*, 5430. <https://doi.org/10.3390/app13095430>

Academic Editors: Wojciech Zgłobicki and Leszek Gawrysiak

Received: 4 April 2023

Revised: 14 April 2023

Accepted: 17 April 2023

Published: 27 April 2023



Copyright: © 2023 by the authors. Licensee MDPI, Basel, Switzerland. This article is an open access article distributed under the terms and conditions of the Creative Commons Attribution (CC BY) license (<https://creativecommons.org/licenses/by/4.0/>).

1. Introduction

In recent years, natural disaster events have become more frequent, including many mega-earthquakes that have caused more serious casualties in combination with climate change [1,2]. According to data published by the United Nations Office for Disaster Risk Reduction (UNDRR), they predicted that more than 750,000 people would be killed in earthquake disasters between 2001 and 2020, accounting for 59% of all disaster deaths. Although scientists have been searching for ways to predict earthquakes, mankind has not yet been able to fully grasp the mechanism of earthquakes and their precursors. Currently, no country in the world can accurately predict earthquakes [3]. Therefore, an accurate emergency response after an earthquake is an effective and critical means of reducing earthquake casualties.

The occurrence of large earthquakes is usually accompanied by the collapse of many buildings and people who are trapped [4]. If emergency rescuers can quickly access trapped people in the disaster area after an earthquake, it can greatly improve the efficiency of emergency rescue and save more lives to a maximum extent. However, after a destructive earthquake, the disaster area often suffers from communication and transportation disruptions and lagging access to disaster information. As a result, rescuers are unable

to accurately understand the distribution and number of trapped people in the disaster area in a timely manner, so the establishment of a scientific and effective pressure burial assessment system is crucial for emergency command decisions [5].

Due to the lack of specific disaster information at the early stage of rescue, some researchers have estimated the degree of damage of buildings according to the level of the earthquake disaster, so as to establish a statistical model to predict the total number of large-scale buried personnel [6,7]. A.W Coburn et al. [8] investigated the relationship between collapsed buildings and human casualties. He et al. [9] achieved a rapid assessment of the post-earthquake blind field by constructing a correlation model between mortality and injury rates and earthquake intensity at different administrative area levels. Freire et al. [10] combined urban population density with seismic hazard rating to derive potential casualties in seismic hazard risk areas for the specific planning of subsequent rescue needs and investigated the relationship between collapsed buildings and human casualties. Feng et al. [11] established an empirical function for earthquake personnel losses, using the relationship between seismic parameters and the number of casualties reported from historical data. So et al. [12] calculated the relationship between multiple earthquake deaths and buildings, and proposed the impact of different building structures on the number of casualties. Xu et al. [13] proposed a method for assessing earthquake crushers based on building collapse, which was based on the relationship between the time of earthquake onset and the number of casualties. Xiao et al. [14] proposed a model for estimating the crush and burial rate with the a priori probability of personnel in terms of the indoor population rate and building collapse rate. Wu Chen et al. [15] analyzed the statistics of the number of casualties of historical earthquakes in China and obtained an empirical pressure burial rate calculation equation based on the building collapse rate. Utilizing remote sensing methods, Ranjbar et al. [16] suggested calculating the number of casualties based on the time of the earthquake, the structural material of each building, and the extent of destruction. Huang et al. [17] proposed a robust wavelet v-SVM earthquake casualty estimation model using multi-source data. These methods mainly focus on the assessment of the number of casualties after the earthquake, and most of the assessment units are at the municipal level, which cannot effectively reflect the regional differences in the distribution of buried personnel and the identification of key areas.

So, the assessment method based on the population kilometer grid is widely used. Yang [18] gave a preliminary method for calculating the number of trapped people in a kilometer grid by fully considering the factors affecting the buried people. Yu et al. [19] programmed and optimized Yang's equation, and the evaluation results analyzed by arithmetic cases can identify where the key areas of buried people are. Zhou et al. [20] combined the kilometer grid data of the Gansu Province with localized parameter improvement for the earthquake formula. The applicability of the pressure buried personnel distribution assessment method for Gansu area was improved. Bai et al. [21] established a model for the number of people buried by earthquakes based on the grid and high-precision house data for the Ludian and Yiliang earthquakes in the Yunnan Province as an example. Bing et al. [22] proposed a method to assess the number of buried people due to building collapse in an earthquake disaster by combining the estimation model of earthquake casualties with the assessment unit of township residential land. Wei et al. [23] established an assessment model for the number of people trapped in collapsed buildings in an earthquake to show the distribution in a kilometer grid distribution as an example of the Ludian earthquake and verified the accuracy of the assessment results.

There have been many studies related to people who are trapped in Table 1, but the existing studies have limitations: (1) The requirement of data in most methods involve a wide range of information and data. These data are costly to obtain and slow to update. Moreover, the lack of such basic data in the currently available emergency database makes the applicability of existing methods insufficient. (2) Existing models that can be used directly are more conducive to estimating the overall casualty situation in the region. Although the km grid method is more refined for personnel buried pressure prediction,

with the development of sensors in aerospace technology and the increasing demand for emergency efficiency, a more refined personnel buried pressure model can be attempted to be constructed, forming the rough prediction of the overall number of people buried pressure in a large range, the prediction of personnel buried pressure in km grid scale, and then the prediction of personnel buried pressure in fine individual buildings. Therefore, this paper proposes an evaluation model of earthquake-trapped personnel using remote sensing images, UAV images, and multi-source geographic data through the simulation of population distribution, the construction of personnel in the indoor population rate, and the degree of building damage after the earthquake to analyze the key rescue areas for emergency rescue work. Finally, this paper uses the town of Moxi, the epicenter of the recent earthquake in Luding, Sichuan, as a case study for experiment and analysis.

Table 1. Modeling and methods approaches.

Estimation Modeling	Methods	References
Seismic-based statistical model	Adding the earthquake-related parameters fitting function to the post-earthquake casualty data	[8–10]
	Adding the material structure and collapse rate of buildings with the post-earthquake casualty data	[11–13,15]
	Based on the prediction model of building collapse rate and chamber rate	[14]
Statistical model based on kilometer grid	Based on multi-source data	[16,17]
	Statistical model was optimized by superimposing multi-source data with kilometer grid as unit	[18–23]

2. Methods

From the point of view of fine rescue, this paper constructs an estimation model of buried personnel in a single building. As illustrated in Figure 1, the model is mainly divided into two stages: “Pre-earthquake Key Information Extraction” and “Post-earthquake Risk Assessment of Seismic People Trapped”.

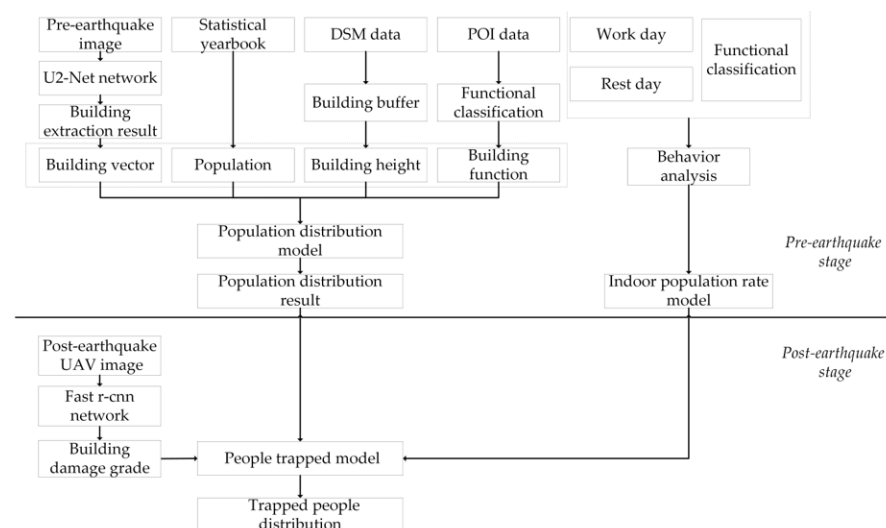


Figure 1. Flowchart of the proposed work.

Pre-earthquake stage is for extraction of the key information factor of people trapped. Pre-earthquake high-resolution satellite imagery is used to obtain building edge information; Point of Interest (POI) data are used to obtain building function; and Digital Surface Model (DSM) data are used to obtain building height information. Statistical yearbooks are used to obtain demographic data for the study area. Based on the information obtained above, we used a “Population Distribution Model” to simulate the distribution of the local

population and to study the indoor population rate assessment under different building attributes and different time periods.

Post-earthquake stage is an estimation of people trapped after earthquake based on multi-source data. Post-earthquake aerial imagery is used to extract the damaged buildings and the results are fed into our proposed single building burial model, as shown in Equation (1), to finely estimate and analyze seismic people trapped in earthquake.

$$B_p = P_i \times P_t \times D_d \quad (1)$$

where B_p represents the estimation number of people trapped in a single building; P_i represents the number of people in a single building; P_t represents indoor population rate; and D_d represents degrees of building damage. It is important to emphasize that the description of trapped people in buildings in this paper does not include those who were quickly removed from danger either by themselves or by mutual rescue. These people may die, be seriously injured, or buried too deeply to save themselves or each other during an earthquake. In this paper, referring to previous research findings on the rate of serious injury and mortality of personnel at different degrees of damage [24–26], the burial rate is taken to be 1/300 in the severely damaged building state and 1/20 in the destroyed building state.

2.1. Pre-Earthquake Phase

2.1.1. Population Distribution

The true spatial distribution of the population should be conducted using a census. However, this approach is both costly and difficult to achieve. To address this issue, this paper explores the intrinsic link between building size, building function, and people distribution, using an area weighting method to refine the population of different age levels to each building. The specific calculation process is shown in Equations (2)–(4).

$$P_i = P1 + P2 \quad (2)$$

$$P1_i = \frac{S}{S_i} \times T \quad (3)$$

$$P2_i = \frac{S}{S_i} \times R \quad (4)$$

In the above equation, P_i stand for the population in the building with function i . $P1$, $P2$, and S , respectively, stand for the resident population, random population, and floor area of the building with function i . S_i , T , and R , respectively, stand for total building area in different functions, total population, and total mobile population under the function of the administrative district where they are located.

Since the population distribution of each building is not counted in most undeveloped areas, we need to simulate the population of each building according to different age groups and different building functions. Firstly, we will simulate the total number of resident staff in buildings with the same function. According to the work of different groups, we will divide them into the following groups: 0–14 years old, 14–60 years old, and over 60 years old, and we will allocate different age groups to the same function according to their functions. For example, the 0–14-year-old group is mainly in education during the day and accommodation at night. In the daytime, the total number of schools is equal to the total number of permanent residents aged 0–14. Then, population distribution of individual buildings is conducted according to Equation (3), which concerns the proportion of each school area to the total area of education services. Through the study of indoor population in Sichuan area [27,28], the functional areas of each age group in different time periods were summarized. Tables 2 and 3 below show the corresponding architectural functions at different ages and times.

Table 2. Different ages on weekdays in the functional area.

Age	8:00–17:30	17:30–22:00	22:00–8:00
0–14	Educational services	Accommodation service Commercial service Leisure service	accommodation service
14–60	Hospital service Livelihood service Enterprise office	Accommodation service Hospital service Livelihood service Commercial service Leisure service Enterprise office Educational services	Accommodation service Leisure service Enterprise office Educational services Tourist attraction
60+	Leisure service Accommodation service Tourist attraction	Livelihood service Accommodation service	Accommodation service
Random population	Tourist attraction	Accommodation service Commercial service Leisure service	Accommodation service Commercial service Leisure service

Table 3. Different ages in the rest weekdays in the functional area.

Age	8:00–17:30	17:30–22:00	22:00–8:00
0–14	Educational services Leisure service Commercial service Accommodation service	Accommodation service Commercial service Leisure service	Accommodation service
14–60	Hospital service Livelihood service Commercial service Leisure service Enterprise office Educational services Leisure service	Accommodation service Hospital service Livelihood service Commercial service Leisure service Enterprise office Educational services	Accommodation service Leisure service Enterprise office Educational services
60+	Accommodation service Tourist attraction	Livelihood service Accommodation service	Accommodation service
Random population	Tourist attraction	Accommodation service Commercial service Leisure service	Accommodation service Commercial service Leisure service

1. Building area S

The content of basic geographic data varies from region to region around the world, and not all regions have real-time updated building mapping data. This paper proposes a method to obtain the area of pre-earthquake buildings based on remote sensing images, with professional manual correction, to form relatively accurate vector data of buildings. The U2-Net network [29] is used to detect building edge information, which is able to capture much contextual information in imagery and increase the depth of the architecture without significantly increasing the computational cost. Vectorization and manual inspection were carried out based on the above results, and the roof area was calculated using the computational geometry function in ArcGIS.

In addition, DSM data are used to obtain the floor height of the building. This method uses the center of the building as a rectangular buffer zone, the plural of DSM points within the building contour as the building elevation, and the plural of DSM points in the non-building area within the buffer zone as the ground elevation, and calculates the number of floors by calculating the building height. The floor height of the building is taken with reference to the Residential Design Code, which depicts the height of ordinary residential floors as 2.6–2.80 m, and the floor height of stores is generally between 4.5 and

5.1 m. Therefore, the height of ordinary residential floors in this paper is set to 2.7 m, and the floor height of stores is set to 4.8 m. Finally, the area of the top surface of the building multiplied by the height of the floor is obtained.

2. Identification of the building function i

As buildings are an important part of cities, the functional classification of urban buildings can provide a favorable basis for the division of urban functional areas, assist government departments in managing and making decisions on the distribution and allocation of urban planning [30–32], land use [33], resources [34], and population [35], and help promote the sustainable development of urbanization construction [36]. In our study, the results of the determination of building function can effectively improve the accuracy of the indoor population rate, and can be effectively applied to the risk assessment of the seismic people trapped.

In this paper, a method of functional classification of buildings based on high-resolution remote sensing imagery is proposed and used. Firstly, the building edge information in the pre-earthquake high-resolution remote sensing images is extracted using deep learning method. Then, the POI data are sorted and classified according to the experimental idea, and finally, the two are fused together to realize the functional judgment and classification of single buildings before a disaster.

There are too many types of POI data, and a single functional building often contains multiple POI points. Consider the similarity of multiple functions, it is necessary to delete and merge POI data. In this paper, according to the Classification Standard of Land Use Status (GB/T21010-2017), building functions are divided into 8 categories, including accommodation service, hospital service, livelihood service, enterprise office, commercial service, tourist attraction, educational service, and leisure service. The data classification results are shown in Figure 2.



Figure 2. POI functional classification.

2.1.2. Indoor Population Rate

The indoor population rate is used to describe the presence of people in a building during a certain period, which involves many factors, such as the specific time of day (day, night, and holidays), weather conditions, occupant density, population size, and the living and production conditions of the residents. In the field of earthquakes, the indoor population rate is mainly related to geographical location, working days and non-working days, age of residents, buildings with different functions, earthquake occurrence time, population structure, and occupation. Of course, some factors are indefinite, such as climatic conditions and interim policies. The occupancy rate is the ratio of the number of people in the building to the accommodated population, and it takes a value in the range of 0–1. In previous studies, the indoor population rate is mostly determined for a specific area based on surveys of local occupancy patterns, requiring significant human and financial resources, which are not universally applicable. Moreover, the indoor population rate with buildings of detailed function has been less studied. To obtain the results of indoor population rate with universal applicability, we studied the results of indoor population rate with universal applicability based on Sichuan population's activity literature [27,28]. The specific relationships are shown in Figures 3 and 4.

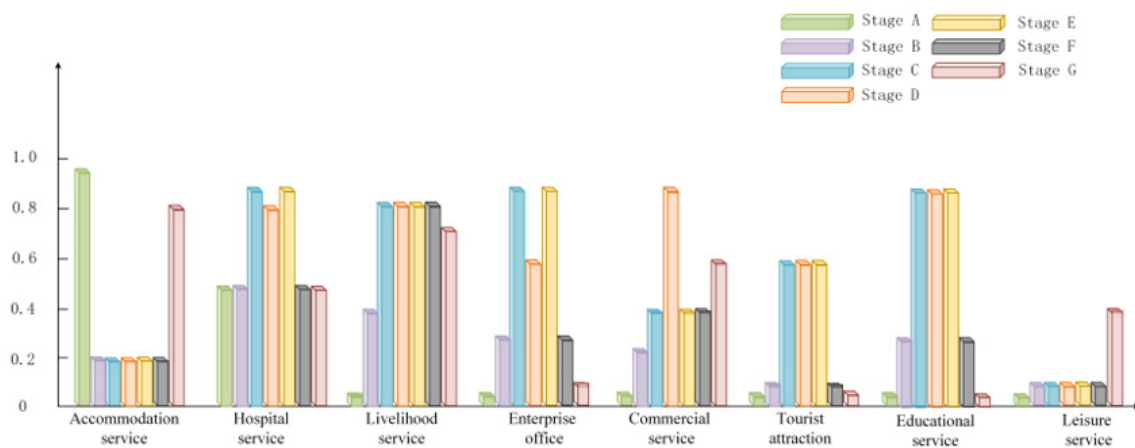


Figure 3. Indoor population rate in workday.

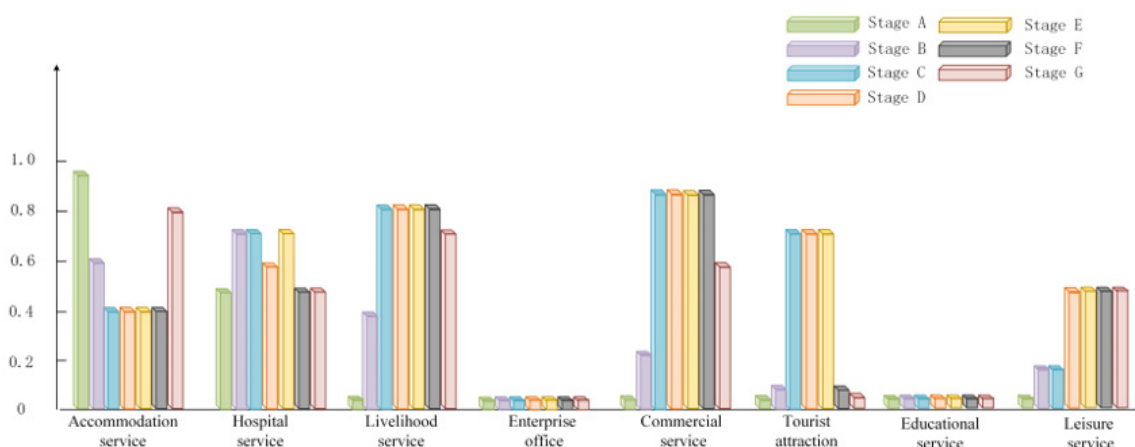


Figure 4. Indoor population rate in rest day.

The indoor population rate is considered to be related to a variety of factors, both definite and indefinite, such as the moment of earthquake, working days or rest days, population size, population structure, occupation, and building function. Individual movements of people are more random, but group population movements have a certain regularity. Each day can be divided into two categories: working day or rest day, and the

24 h day can be divided into 7 periods. Stage A stands for sleep period (22:00 the previous day to 06:30 the next day). Stage B stands for morning commute (06:30–08:00). Stage C stands for working period (08:00–12:00). Stage D stands for rest period (12:00–13:30). Stage E stands for working period (13:30–17:30). Stage F stands for evening commute (17:30–19:00). Stage G stands for rest period (19:00–22:00).

By analyzing the behavioral characteristics of the population at various times of the work and rest day, the economic census data are combined to quantify the indoor population rate. The social activity patterns of the various sectors and the indoor population rate of the functional buildings are summarized in this study. The indoor population rate of each functional building on working days is shown in Figure 3 and the indoor population rate of each functional building on rest days is shown in Figure 4.

For buildings with weekday accommodation service, the indoor population rate is 0.95 in stage A, when the population is basically asleep. In stages B–F, during working hours, only the elderly and young children (0–2 years old) are present in buildings with this function, so the indoor population rate is 0.2. In stage G, when the population is resting at home after work, the indoor population rate takes 0.8. For buildings with a rest day accommodation service, the indoor population rate is still 0.95 in stage A. In stage B and G, there are trips, so the indoor population rate is 0.6. In stages C–F, there are generally home and travel behaviors, so the indoor population rate is taken as 0.4.

The hospital service is divided into inpatient and outpatient, with medical and nursing staff, outpatients, inpatients, and escorts during daytime, and inpatients, escorts, and medical and nursing staff on duty at night. Therefore, the indoor population rate of stage A, B, F, and G is basically the same as 0.5. The indoor population rate of stage C and E is 0.9 for working hours. During lunch break, medical and nursing staff and accompanying staff are out, so the indoor population rate of D is 0.7. On rest days, the general number of medical and nursing staff is reduced, and the general number of patients remains unchanged, so 0.5 is the indoor population rate of stages A, B, F, and G. A score of 0.8 is used as the indoor population rate of stages C and E for working hours, and 0.6 is used for the indoor population rate of stage D.

Livelihood service is mainly for public facilities, transportation facilities, and other services. Staff need to serve the residents, so their work time is earlier than the company enterprise. Additionally, their off-time is later than the company's. So the indoor population rate of stage A is taken as 0.05. The indoor population rate of stages B, F, and G is 0.7. The indoor population rate of stages C–E is 0.9. The rest days are generally taken as the same value.

The travel time of enterprise office on weekdays is concentrated; stage A and G are off-duty rest time, due to the duty and property staff, and the indoor population rate is 0.05. In stages B and F, most people commute, and so the indoor population rate is 0.3. There are a few office workers in stages C and stage E, and so the value is 0.9. Stage D includes catering and leisure, and so the value is 0.6. All rest days are taken as 0.05.

Commercial service operations are usually slightly later than corporate offices. The indoor population rate of stage A is 0.05. The indoor population rate of stage B is 0.3. The indoor population rate of stage C and E businesses is less, at 0.4. Stage E time is more concentrated for the passenger, so the indoor population rate is 0.9. Stage G time gradually decreases for the passenger, so the indoor population rate is 0.6. Rest day commercial service traffic is more, and therefore, the rate of stage A is 0.05. The indoor population rate of stage B is 0.3. The traffic is more concentrated in the stage C–F periods, and the indoor population rate is 0.9. The traffic decreases gradually in the stage G period, and the indoor population rate is 0.6.

The general traffic flow of tourist attractions on weekdays is concentrated in stage C–E time periods, and the indoor population rate is 0.6. Stages B and F gradually decrease, and the indoor population rate is 0.2. Stages A and G are in the scenic area closed states, and the indoor population rate is 0.05. The traffic flow of rest days is surplus to weekdays, and so for stage C–E time periods, the indoor population rate is 0.8. Stages B and F gradually

decrease, and the indoor population rate is 0.2. Stages A and G are in the scenic area closed states, and the indoor population rate is 0.05.

Educational services are mainly for kindergartens, elementary school, and secondary schools. The indoor population rate of stages A and G on weekdays is 0.05. Stages B and F are for commuting time, and the indoor population rate is 0.1. Stages C–E are for the school period, and the indoor population rate is 0.9. All stages are 0.05 during the rest days.

Leisure service weekday traffic focuses in the off-hours, so the indoor population rate of stage A is 0.05. The indoor population rate of stages B–F is 0.1. After a gradual increase in personnel after work, the indoor population rate of stage G is 0.4. R = When rest day traffic increases, which is generally concentrated in stages D–G, then the indoor population rate is 0.6. When stages B and C number are less, then the indoor population rate is 0.2. The indoor population rate of stage A is 0.05.

2.2. Post-Earthquake Phase

Damage class classification guidelines have been proposed for building damage assessment [37]. For remote sensing assessment, some detailed wall damage and structural damage are difficult to detect in most existing guidelines for classifying damage levels in remote sensing images. As shown in Table 4, we classified buildings into only three classes for emergency remote sensing assessment after earthquakes compared to the European Large Earthquake Scale (EMS98) [38]. The differences of buildings with almost undamaged grade, partial collapse grade, and damage grade in remote sensing images can be seen in Figure 5.



Figure 5. Building damage grade.

Table 4. Building damage grade of the remote sensing image.

EMS98		Ours	
Grade Name	Description	Grade Name	Description
Negligible to slight damage	No structural damage; slight non-structural damage	Almost undamaged	The structure of the building is complete, and the main structure has not collapsed or partial collapse
Moderate damage	Slight structural damage; moderate non-structural damage	Partial collapse	Partial collapse of the building, or partial damage to the roof, or damage to the parapet; 10–50% deformation
Substantial to heavy damage	Moderate structural damage; heavy non-structural damage		
Very heavy damage	Heavy structural damage; very heavy non-structural damage		
Destruction	Very heavy structural damage	Damaged	The whole building collapsed completely, or the roof collapsed completely, or more than 50% of the main structure collapsed with overall distortion, deformation, or tilt

Since post-earthquake detection requires a fast and accurate method, this paper uses the method of Fast r-cnn [39] for building damage, and extracts the center point of the rectangular box as the result of building damage grade, and then aligns the center point as a vector that is superimposed on the building vector layer.

3. Study Area and Data

3.1. Study Area Profile

The seismic event studied here is the 2022 Luding earthquake in Sichuan, China. An Ms 6.8 earthquake occurred in Luding County, Ganzi Tibetan Autonomous Prefecture, Sichuan Province, with a depth of 16 km on Monday, 5 September, at 12:52 a.m. The earthquake killed 97 people, 21 people were lost, and 423 people were injured (including 6 critically injured and 42 seriously injured). The earthquake reached a maximum intensity of 9 degrees, resulting in a higher number of casualties and severe damage to infrastructure and houses compared to earthquakes of the same intensity [40]. The victim area mainly involves seven townships in Luding County, Ganzi Tibetan Autonomous Prefecture, such as Moxi town, Detou town, Yanzigou town, and Dewei town. In this paper, the township site of the extremely hard-hit area of Luding earthquake, the township of Moxi, is selected as the experimental area, covering 3.5 km² area of Vaihingen. The model construction of post-earthquake personnel burial pressure is based on multi-source data.

3.2. Data Descriptions

According to the experimental idea and techniques, the pre-earthquake images were acquired by Google Earth service; the post-earthquake images were acquired by a small unmanned aerial vehicle (UAV). In addition, this research paper used some other types of auxiliary data such as POI (Point of Information). The details of the data used in this paper are shown in Table 5.

Table 5. Description of the data used in the study.

Data Type	Acquisition Time	Source	Spectral Band	Spatial Resolution
Pre-earthquake image	April 2021	Google Earth	RGB	0.6 m
Post-earthquake image	September 2022	UAV	RGB	0.1 m
DSM data	May 2021	National Earthquake Response Support Service	-	0.1 m
POI data	April 2022	AMap	-	-
Population statistics	December 2021	Statistical Yearbook	-	-

4. Experimental Results

4.1. Building Extraction Results

In this paper, the U2-Net network uses 3600 samples (512×512) as the training set, 1200 samples (512×512) as the validation set verification set, and 1200 samples (512×512) as the prediction set. Its hyper parameters are set to default (initial learning rate $lr = 1 \times 10^{-4}$, $\text{betas} = (0.9, 0.999)$, $\text{eps} = 1 \times 10^{-8}$, $\text{weight decay} = 0$, $\text{epoch} = 350$). Its extraction results are shown in Figure 6. *Precision*, *Recall*, *F1-Score*, and *IoU* as accuracy indicators are selected for verification, where *Precision* reaches 75.45%, *Recall* reaches 62.54%, *F1-Score* reaches 68.39%, and *IoU* reaches 56.58%. From the results, the U2-Net network model detection results can reduce the workload of manual vectorization and improve the efficiency. The data in the red box in Figure 6 (the township site of Moxi) are of a densely built-up area, which is used in the later experiment.

$$\text{precision} = \frac{TP}{TP + FP} \quad (5)$$

$$\text{Recall} = \frac{TP}{TP + FN} \quad (6)$$

$$\text{F1-Score} = 2 \times \frac{\text{precision} \times \text{Recall}}{\text{precision} + \text{Recall}} \quad (7)$$

$$\text{IoU} = \frac{Ap \cap Ar}{Ap \cup Ar} \quad (8)$$

where *TP* denotes the area of correctly predicted buildings. *FP* and *FN* are the mispredicted correct and incorrect areas of the buildings. *Ap* and *Ar* represent the predicted and true areas of buildings, respectively, in each damage grade.

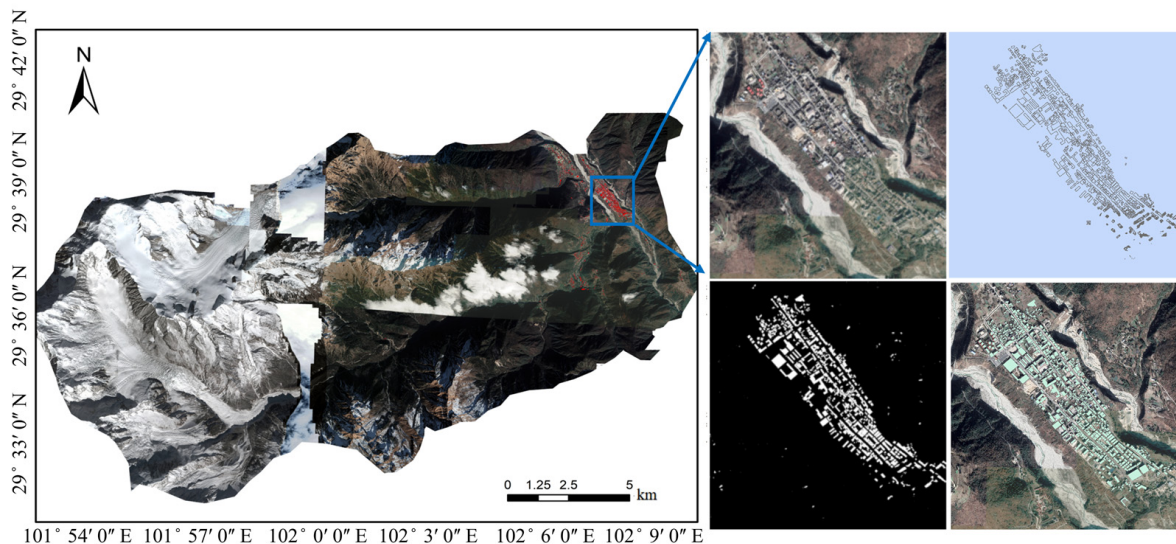


Figure 6. Building extraction and vectorization results.

4.2. Building Function Identification Results

From the results as shown in Figure 7, the accommodation services including the residential and hotel are relatively large in the town of Moxi, and the commercial services are also more developed, which is in line with the functions of the tourism industry in Moxi.

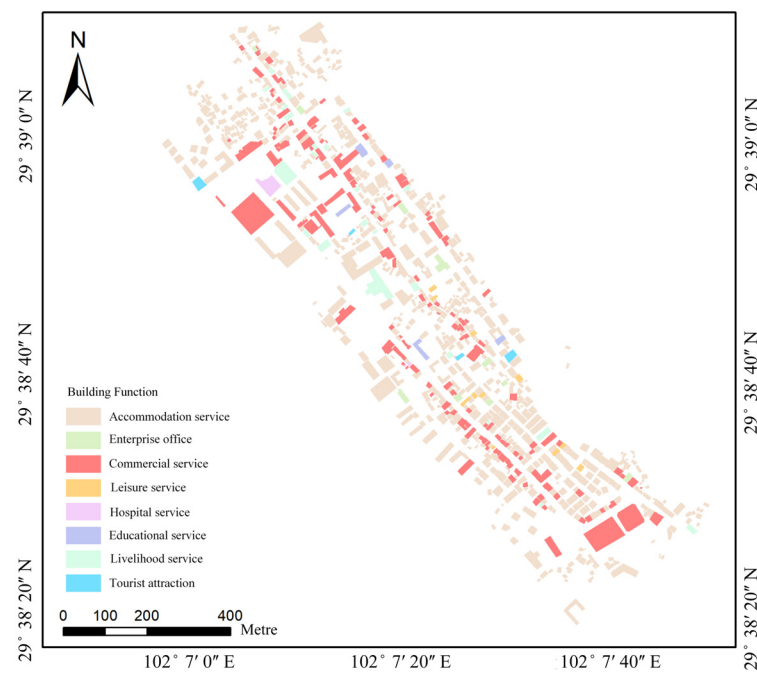


Figure 7. Building function identification results.

4.3. Building Floors Number Results

The results of the building floor number determined using DSM are shown in Figure 8. From Figure 8, there are few high-rise buildings in the site of Moxi town, and the floor height is generally lower than four stories.

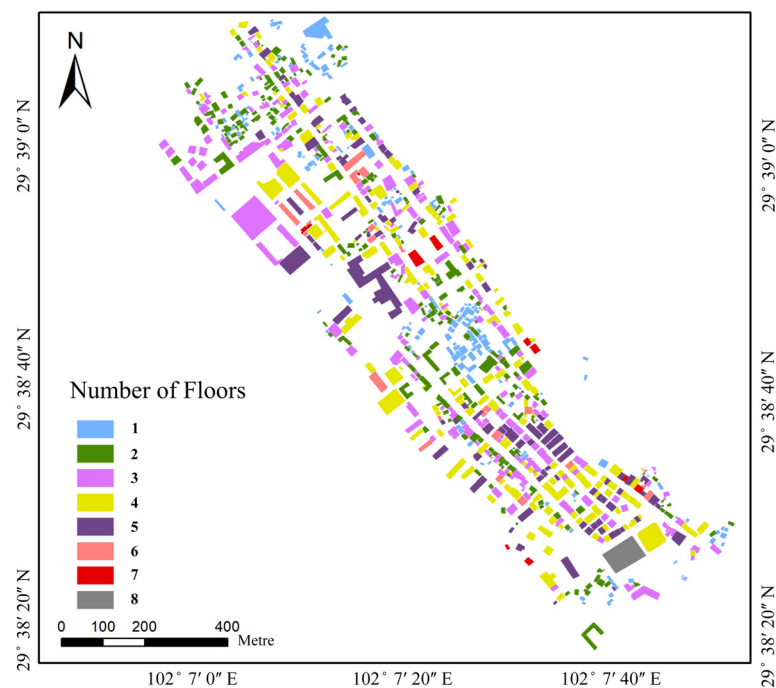


Figure 8. Building floors number results.

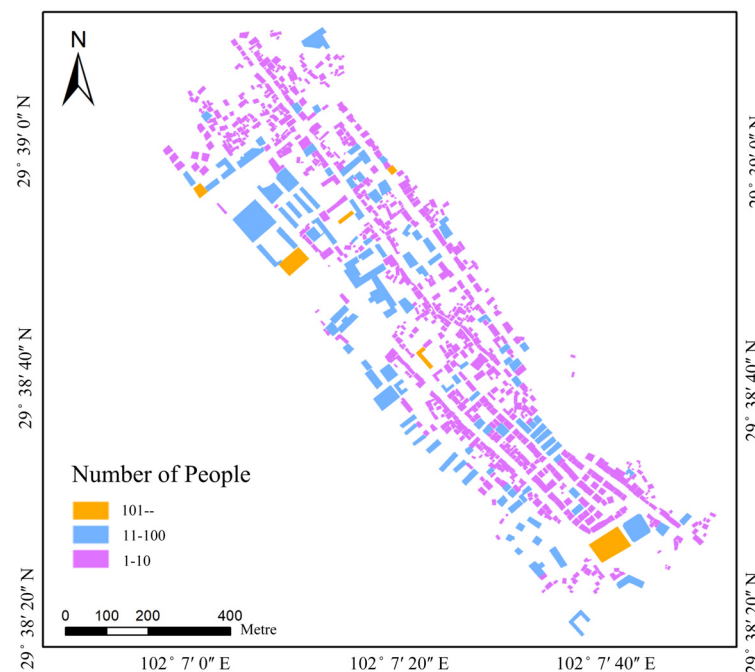
The floor area of the building can be calculated using the number of floors. The number of buildings and the overall area are counted, and the results are shown in Table 6.

Table 6. Buildings and overall area statistics.

Building Function	Number	Total Area (m ²)
Accommodation service	745	500,406.91
Hospital service	5	7988.28
Leisure service	10	8468.25
Livelihood service	24	41,733.30
Enterprise office	12	13,515.43
Commercial service	157	229,199.30
Tourist attraction	3	4704.00
Educational services	5	6924.99
Total	961	812,940.46

4.4. The Rural–Urban Population Results

According to the Luding Statistical Yearbook, the rural–urban population of the township of Moxi is 3131, of which 16.54% are aged 0–14, 65.53% are aged 15–59, and 17.93% are aged 60 or older. Due to the epidemic control, the floating population consists of about 300 people, who are mainly tourists. The results of their population distribution are shown in Figure 9. In the experimental area, the building has a population of more than 100 people and its main functions are business, accommodation services, educational services, and tourist attractions. Functions of 10–100 people buildings include accommodation services (78.4%), commercial services (14.8%), livelihood services (3.4%), educational services (2.3%), and hospital services (1.1%). Before obtaining post-earthquake images, the detailed damage situation of buildings cannot be known. Therefore, when remote sensing images are not acquired after the earthquake, the focus should be on the accommodation services, commercial services, education services, and tourist attractions in the area.

**Figure 9.** Estimated population distribution results by the proposed method.

4.5. Test Results of Damaged Buildings

The buildings were extracted using the Fast r-cnn network in the post-earthquake phase. The paper sketched 1000 samples of VOC (512×512) for training, accounting for about half of the images, and the other half for testing ($lr = 1 \times 10^{-3}$, epoch = 300), if the intersection-over-union between the ground truth annotation and the predicted bounding

box is greater than 0.5. The building damage results are shown in Figure 10. The results are shown in Table 7. The resulting centroid vectorization is then superimposed on the pre-earthquake building vector layer. The results are shown in Figure 11. The building damage rate is high, which is in accordance with the findings in the literature [32].

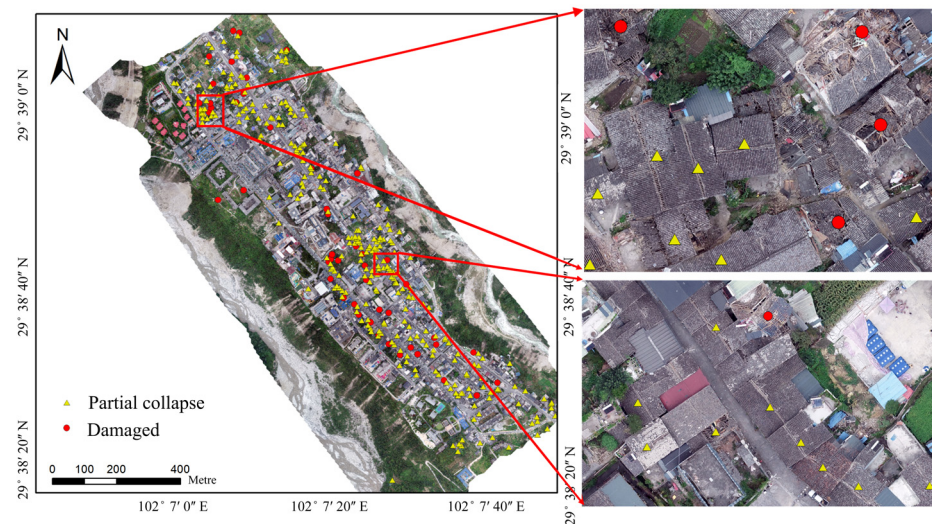


Figure 10. Building damage grade and zoomed results.

Table 7. Buildings damage grade accuracy evaluation.

Buildings Damage Grade	Damaged	Partial Collapse
<i>TP</i>	43	240
<i>FN</i>	6	15
<i>FP</i>	8	12
<i>Precision</i>	84.31%	95.23%
<i>Recall</i>	87.76%	94.12%
<i>F1-Score</i>	86.50%	94.67%

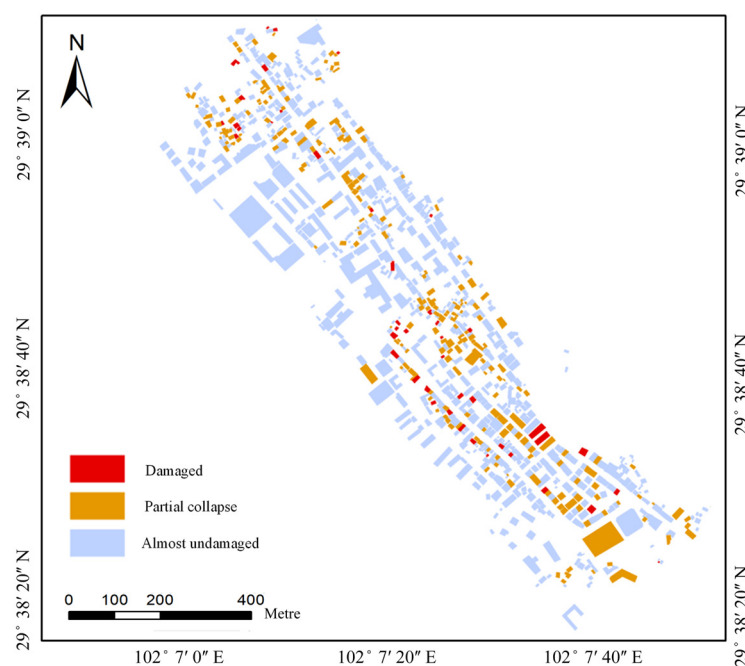


Figure 11. Building damage grade results.

4.6. Estimation and Analysis of People Trapped

The overall number of people trapped was estimated to be four persons according to the burial equation for building burial. Since no specific trapped personnel location data are available for verification, casualty rates are used for verification. Following the method of Yin [41], one person was calculated as dead and fourteen were injured using the population distribution and the degree of building damage method above. The results are consistent with the detailed actual death toll statistics of the Luding earthquake [40].

In this paper, although the building damage reached nearly 300 buildings, only four people were buried. The overall search and rescue without weighting will delay the rescue efficiency. This paper uses the refinement buried population model to estimate the probability number of buried people in each building in the area in Figure 12. Rescue priorities can be derived, such as the red building's search and rescue priority being the highest, the yellow and blue areas being second, and the green building personnel being safer, which can improve the efficiency of the rescue.

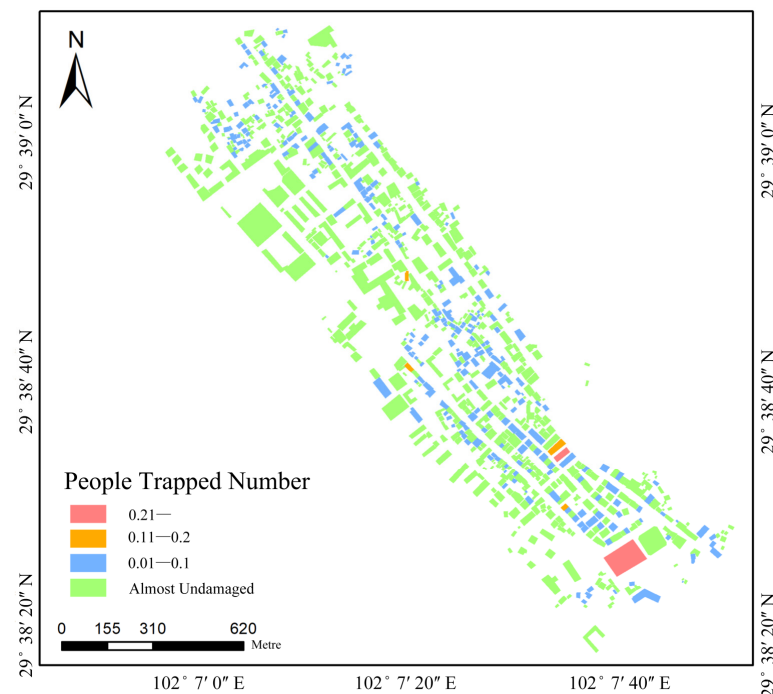


Figure 12. Number results of people trapped.

5. Discussion

5.1. Data Accessibility

The multi-source data acquisition for this article is easy. The required data is detailed below. In the study, the use of remote sensing images with low cloud noise and close time before earthquakes is something that should be considered. DSM data can be extracted by remote sensing technology using high spatial resolution satellites and UAV. POI data exist in software such as Baidu Map and AMap. Population data are generally available from local government statistics. Post-earthquake images are selected from UAV with high timeliness. Hence, the data involved in the proposed method are relatively easy to obtain. The data can be applied to most of the geographical areas, unlike the other methods, which require precise data from manual research.

5.2. Effectiveness of the Method

The most critical phase of the rescue operation concerns the determination of the number of casualties and their exact distribution in the aftermath of the earthquake. This

problem will help managers to deploy rescue personnel in a rational manner. The overall number of casualties estimated with the model in this paper is basically consistent with the actual number of casualties. At the same time, compared with large-scale people trapped models, the rescue target estimated by the model is clearer, and the number of trapped people in each building can be assessed, which is more in line with the need for accurate rescue in modern emergency rescue operations.

5.3. Time Efficiency of the Method

All the experiments are implemented on an NVIDIA Geforce RTX 3060 12-GB GPU. The approach in this paper is divided into two phases in Figure 13, where building extraction and damage detection do not include training time. The first stage is the pre-earthquake stage, which takes 195 min. The second stage is the post-earthquake stage, which based on the acquired images; the building damage detection and center point vectorization take 20 min, and the buried distribution of people takes 30 min.

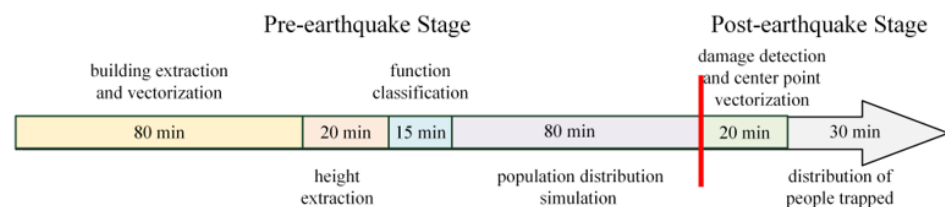


Figure 13. Time efficiency of the method.

The overall time spent is about 245 min, which meets the requirement of 72 h of rescue. The pre-earthquake phase takes a long time, but it can simulate the results in advance. In the pre-earthquake, relevant information can be extracted in advance to improve the efficiency of the personnel buried pressure model. The post-earthquake phase requires remote sensing images of earthquakes that have already occurred and cannot be predicted in advance. So, the length of the post-earthquake phase cannot be shortened.

6. Conclusions

This paper proposes a rapid assessment method for the distribution of trapped personnel for earthquake emergency rescue work. Compared with previous studies, the contributions of this paper are as follows: (1) A refined assessment of a people trapped model is proposed. The method considers multiple factors, such as the population distribution, presence rate, and degree of damage, to estimate the number and distribution of buried people in a single building, which ensures that the estimated number of people trapped is relatively accurate. So, the proposed method can effectively guide the recommendations and strategies for earthquake emergency rescue. (2) The proposed method is suitable for implementing a dynamic assessment of personnel distribution over time and expressing the differences in population distribution due to population mobility, and thus, it can potentially provide optimization on the timescale for the assessment of the distribution of personnel trapped by earthquakes.

In summary, the trapped personnel estimation model in this paper is a promising and refined workflow. Through the analysis of the personnel distribution in different areas, the densely populated earthquake evacuation area is planned in different time periods. According to the results of the building damage detection, the seismic resistance and aging degree of the damaged buildings in the area can be investigated on the spot, and buildings with the same seismic resistance and aging degree that were not damaged in this earthquake can be reconstructed to withstand the damage of future seismic events.

This article has some shortcomings; for example, the personnel presence rate is closely related to season, weather, and temporary policies. Therefore, more factors need to be considered in further research. In the next research plan, we will consider the influence of weather on the room rate, including the influence of extreme weather such as rain, snow,

and sand storms on the room rate. Considering the influence of seasons, for example, the room rate of people going out at night in the winter increases, while the room rate of people at night in the summer is low. This part of the work also needs to be refined in response to the differences in the morphology of the building structure at the time of damage and the similar differences in the burial rate. Meanwhile, smartphone data can be used to simulate population distribution as well as detect anomalies after earthquakes [42,43]. With the development of smartphones, this will become a trend.

Author Contributions: Conceptualization, S.X., J.Y. and D.M.; data supplement, J.Y.; methodology, S.X. and H.Y.; experiments and validation, S.X. and R.L.; funding acquisition, D.M.; writing, S.X. and Z.Z. All authors have read and agreed to the published version of the manuscript.

Funding: This research has been jointly supported by the National Key R&D Program of China (2022YFB3903604) and the Fundamental Research Funds for the Central Universities (AR2212).

Institutional Review Board Statement: Not applicable.

Informed Consent Statement: Not applicable.

Data Availability Statement: Not applicable.

Conflicts of Interest: The authors declare no conflict of interest.

References

1. Zhou, L.; Wu, X.; Xu, Z.; Fujita, H. Emergency decision making for natural disasters: An overview. *Int. J. Disaster Risk Reduct.* **2018**, *27*, 567–576. [CrossRef]
2. UNDRR. Annual Average Number of Deaths by Disaster Type. Available online: <https://www.undrr.org/> (accessed on 15 February 2023).
3. Kahandawa, K.A.R.V.D.; Domingo, N.D.; Park, K.S.; Uma, S.R. Earthquake damage estimation systems: Literature review. *Procedia Eng.* **2018**, *212*, 622–628. [CrossRef]
4. Karimzadeh, S.; Miyajima, M.; Hassanzadeh, R.; Amiraslanzadeh, R.; Kamel, B. A GIS-based seismic hazard, building vulnerability and human loss assessment for the earthquake scenario in Tabriz. *Soil. Dyn. Earthq. Eng.* **2014**, *66*, 263–280. [CrossRef]
5. Fawcett, W.; Oliveira, C.S. Casualty Treatment after Earthquake Disasters: Development of a Regional Simulation Model. *Disasters* **2010**, *24*, 271–287. [CrossRef]
6. Yan, D.; Gaozhong, N.; Guiwu, S.U. Construction of an index system for evaluating earthquake emergency response ability of counties. *J. Catastrophology* **2010**, *25*, 125–129.
7. Hu, W.H.; Song, L.J.; Miao, C.G.; Hou, J.S.; Yuan, Z.X. Research on Methods for Classification of Earthquake Stricken Areas and Sequencing of Disaster Degrees—Taking M8.0 Wenchuan Earthquake as an Example. *J. Catastrophology* **2010**, *25*, 30–35.
8. Coburn, A.W.; Pomonis, A.; Sakai, S.; Spence, S.R. Assessing human casualties caused by building collapse in earthquakes. In *Summa-Ries of the International Conference on the Impact of Natural Disasters*; University of California: Los Angeles, CA, USA, 1991.
9. Jun, H.; Shijun, C.; Ruiqing, K. The Out-Sift Rapid Assessment System of Earthquake Disaster and its Application. *Inland. Earthq.* **1998**, *3*, 234–241.
10. Freire, S.; Aubrecht, C. Integrating population dynamics into mapping human exposure to seismic hazard. *Nat. Hazards Earth Syst. Sci.* **2012**, *12*, 3533–3543. [CrossRef]
11. Feng, T.; Hong, Z.; Wu, H.; Fu, Q.; Wang, C.; Jiang, C.; Tong, X. Estimation of earthquake casualties using high-resolution remote sensing: A case study of Dujiangyan city in the May 2008 Wenchuan earthquake. *Nat. Hazards* **2010**, *69*, 1577–1595. [CrossRef]
12. So, E.; Spence, R. Estimating shaking-induced casualties and building damage for global earthquake events: A proposed modelling approach. *Bull. Earthq. Eng.* **2013**, *11*, 347–363. [CrossRef]
13. Xu, J.; Wei, F.; Zhang, L.; Fang, H.; Li, H. Preliminary study on evaluating the number of casualties and trapped victims by a earthquake—A case study of Zhangzhou City, Fujian Province. *J. Seismol. Res.* **2008**, *31*, 382–387.
14. Xiao, D.; Huang, D.; Chen, W. Prediction model for buried personnel probability in earthquake. *J. Southwest. Jiaotong Univ.* **2009**, *44*, 574–579.
15. Wu, C.; Yin, H.T.; Wu, C.; Yin, H.T.; Sun, Q.W.; Zhang, H.; Li, X.; Dong, X.N. Study on the feasibility of the search and rescue information system based on Arcgis. *Plateau Earthq. Res.* **2011**, *23*, 54–59.
16. Ranjbar, H.R.; Dehghani, H.; Ardalan, A.R.A.; Saradjian, M.R.A. GIS-based approach for earthquake loss estimation based on the immediate extraction of damaged buildings. *Geomat. Nat. Hazards Risk* **2017**, *8*, 772–791. [CrossRef]
17. Huang, X.; Zhou, Z.L.; Wang, S.L. The prediction model of earthquake casualty based on robust wavelet v-SVM. *Nat. Hazards* **2015**, *77*, 717–732.
18. Mingru, Y. Study on The Assessment Method of Buried Personnel Distribution in Earthquake. Master's Thesis, Institute of Engineering Mechanics, Harbin, China, 2014.

19. Yu, S.Z.; Zhang, L.X.; Yang, M.R. Assessment of buried people distribution after earthquake. *Earthq. Eng. Eng. Dyn.* **2015**, *35*, 138–143.
20. Zhou, Z.; Chen, W.; He, S.; Sun, Y.; Li, W. Application and Evaluation on a Evaluating Method for Distribution of Earthquake Buried Personnel Based on Population Kilometer Grid: Taking Minxian-Zhangxian M6.6 Earthquake as an Example. *J. Seismol. Res.* **2019**, *42*, 288–294+306.
21. Bai, X.F.; Dai, Y.Q.; Ye, L.Y.; Li, C. Assessment Models of Trapped-victim in Earthquake & Emergency Rescue Area Based on High-precision Building and Population Data. *J. Disaster Prev. Reduct.* **2018**, *34*, 1–12.
22. Wu, B.; Li, Z.Q.; Qi, W.H.; Yang, F.; Li, X.L.; Liu, Y.H.; Fu, B. Trapped Population Distribution in Earthquake and Rescue Policy Based on Township Residential Area Scale: A Case Study of Urumqi Area. *North. China Earthq. Sci.* **2017**, *35*, 13–19.
23. Wei, B.; Nie, G.; Su, G.; Sun, L.; Bai, X.; Qi, W. Risk assessment of people trapped in earthquake based on km grid: A case study of the 2014 Ludian earthquake, China. *Geomat. Nat. Hazards Risk* **2017**, *8*, 1289–1305. [\[CrossRef\]](#)
24. Gutiérrez, E.; Taucer, F.; De Groeve, T.; Al-Khudhairy, D.H.A.; Zaldivar, J.M. Analysis of worldwide earthquake mortality using multivariate demographic and seismic data. *Am. J. Epidemiol.* **2005**, *161*, 1151–1158. [\[CrossRef\]](#)
25. Abeling, S.; Horspool, N.; Johnston, D.; Dizhur, D.; Wilson, N.; Clement, C.; Ingham, J. Patterns of Earthquake-Related Mortality at a Whole-Country Level: New Zealand, 1840–2017. *Earthq. Spectra* **2019**, *36*, 138–163. [\[CrossRef\]](#)
26. Alexander, D.; Magni, M. Mortality in the L'Aquila (Central Italy) Earthquake of 6 April 2009. *PLoS Curr.* **2013**, *5*, e50585b8e6efd1. [\[CrossRef\]](#)
27. Tian, L.L. Analysis of Influencing Factors of Casualties in Earthquake Disaster and the Formula for Estimating Casualties. Graduate Thesis, Capital University of Economics and Business, Beijing, China, 2012.
28. Chen, F. Research on Earthquake Casualty Assessment Method and Program Implementation. Graduate Thesis, Xi'an University of Architecture & Technology, Xi'an, China, 2016.
29. Qin, X.; Zhang, Z.; Huang, C.; Dehghan, M.; Zaiane, O.R.; Jagersand, M. U2-Net: Going deeper with nested U-structure for salient object detection. *Pattern Recognit.* **2020**, *106*, 107404. [\[CrossRef\]](#)
30. Liu, K.; Yin, L.; Lu, F.; Mou, N. Visualizing and exploring POI configurations of urban regions on POI-type semantic space. *Cities* **2020**, *99*, 102610. [\[CrossRef\]](#)
31. Yue, Y.; Zhuang, Y.; Yeh, A.G.-O.; Xie, J.-Y.; Ma, C.-L.; Li, Q.-Q. Measurements of POI-based mixed use and their relationships with neighbourhood vibrancy. *Int. J. Geogr. Inf. Sci.* **2017**, *31*, 658–675. [\[CrossRef\]](#)
32. Cai, L.; Xu, J.; Liu, J.; Ma, T.; Pei, T.; Zhou, C. Sensing multiple semantics of urban space from crowdsourcing positioning data. *Cities* **2019**, *93*, 31–42. [\[CrossRef\]](#)
33. Zhang, T.; Sun, L.; Yao, L.; Rong, J. Impact analysis of land use on traffic congestion using real-time traffic and POI. *J. Adv. Transp.* **2017**, *2017*, 7164790. [\[CrossRef\]](#)
34. Andrade, R.; Ana, A.; Carlos, B. POI mining for land use classification: A case study. *ISPRS Int. J. Geo-Inf.* **2020**, *9*, 493. [\[CrossRef\]](#)
35. Gao, S.; Krzysztof, J.; Helen, C. Extracting urban functional regions from points of interest and human activities on location-based social networks. *Trans. GIS* **2017**, *21*, 446–467. [\[CrossRef\]](#)
36. Hoffmann, E.J.; Wang, Y.; Werner, M.; Kang, J.; Zhu, X.X. Model Fusion for Building Type Classification from Aerial and Street View Images. *Remote Sens.* **2019**, *11*, 1259. [\[CrossRef\]](#)
37. Cotrufo, S.; Sandu, C.; Tonolo, F.G.; Boccardo, P. Building damage assessment scale tailored to remote sensing vertical imagery. *Eur. J. Remote Sens.* **2018**, *51*, 991–1005. [\[CrossRef\]](#)
38. Grünthal, G. *European Macroseismic Scale 1998: EMS-98*; GFZ: Potsdam, Germany, 1998.
39. Girshick, R. Fast r-cnn. In Proceedings of the International Conference on Computer Vision, Santiago, Chile, 13 December 2015.
40. Xu, J.; Zhao, X.H.; Zhou, Q.; Xiao, B.F.; Mao, L.; Xiao, S.L.; Zhou, Y. Casualty study of the Luding, SiChuan M6.8 earthquake. *J. Seismol. Res.* **2023**, 1–12. [\[CrossRef\]](#)
41. Yin, Z.Q. *Prediction Method of Earthquake Disaster and Loss*; Earthquake Publishing House: Beijing, China, 1995.
42. Krichen, M. Anomalies Detection Through Smartphone Sensors: A Review. *IEEE Sens. J.* **2021**, *21*, 7207–7217. [\[CrossRef\]](#)
43. Liu, G.; Onnela, J.-P. Online Anomaly Detection for Smartphone-Based Multivariate Behavioral Time Series Data. *Sensors* **2022**, *22*, 2110. [\[CrossRef\]](#)

Disclaimer/Publisher's Note: The statements, opinions and data contained in all publications are solely those of the individual author(s) and contributor(s) and not of MDPI and/or the editor(s). MDPI and/or the editor(s) disclaim responsibility for any injury to people or property resulting from any ideas, methods, instructions or products referred to in the content.